Ultrawide-Band Modeling of Transient Radiation From Aperture Antennas

Gaetano Marrocco, *Member, IEEE,* and Matteo Ciattaglia, *Student Member, IEEE*

***Abstract*—A new method for the numerical calculation of transient field radiated through aperture-type antennas (slot, open-ended waveguide, and horn) is described. The finite-difference time-domain method is applied for the near-field prediction in the close surrounding of the antenna and a proper data-fitting procedure of the aperture field, involving interpolating functions with separation of space- and time dependence, permits: 1) to calculate "off-line" the radiated field without the need to store a great amount of data; 2) to avoid, in the case of far field, the numerical evaluation of radiation integral; and 3) to obtain approximate far field formulas which are still separable with regard to space and time. The method enables a full data reusability in calculation of field pattern over a wide angular range at a same time, or of the transient response at fixed observation points.**

***Index Terms*—Aperture antenna, finite-difference time-domain (FDTD) analysis, time-domain analysis.**

I. Introduction

DESIGN of ultrawide-band antennas for modern applications [1] in communications, measurements and radar identification and imaging requires to exploit true time domain electromagnetic models. The finite-difference time-domain (FDTD) method combined with the transient near to far (N2F) field transformation [2], [3], which involves the processing of tangential field over a surface enclosing the antenna, is a natural tool for the analysis of real structures with real signals. The application of these methods undergoes some critical aspects. Interpolations over spatial and temporal variables and time buffers are required, during FDTD calculation, to comply with the field staggering within the elementary cell and with the delay time from each surface point source to the observation points. "Off-line" processing, e.g., the N2F transformation after the FDTD run has finished, is generally forbidden due to the not manageable amount of data produced by the transient near field storage. Moreover, spatial and temporal variables are strongly coupled by radiation integrals and a new numerical evaluation is required for each observation time and observation point. For these reasons, time domain N2F is mainly used to calculate the time-domain far-field response at a limited number of observation points, to be defined before the FDTD computation starts.

In recent papers, new approaches have been presented to overcome some of the above method drawbacks. In [4] the multipole expansion is proposed where the weighting coefficients are computed in the time domain by the enforcement of boundary conditions. A rather different algorithm has been presented in [5] which employes a system identification method to extrapolate transient far field at each observation point. Finally, the simplification of the N2F transformation in the case of radiation from apertures on an infinite screen is described in [6] involving the only electric field processing. In the same paper, wavelet analysis has been used to compress time domain data at each aperture point.

This paper proposes a new numeric approach for the approximate transient characterization of aperture antennas, such as slots, open-ended waveguides and horns, which allows the N2F to be calculated off-line without the need to store a great amount of data, to avoid time-consuming evaluations of radiation integral and to obtain far field formulas which are separable with regard to space and time. The latter feature permits a full data reusability in calculation of field pattern. The new method is based on previous papers of the authors [7], [8] concerning the broadband radiation from cavity backed aperture antennas by the *Modal* N2F field transformation in the frequency domain. By a data fitting strategy, the aperture field distribution is approximated by means of summation over suitable space- and time-variant basis functions which simplify the application of N2F. The expansion coefficients are computed in the time domain, during the FDTD run. This method will be now extended to time domain radiation and it will be demonstrated how the radiation integral strongly simplifies, even in the near field, while for far field observation it can be calculated by simple analytical forms for both rectangular and circular apertures. Feasibility and accuracy of the new method will be discussed by application to a rectangular slot antenna and to a true broadband circular ridged horn.

II. Statement of the Problem

Assume that the antenna near field has been computed, for a given excitation signal, by a suitable numerical electromagnetic method within a limited space region [Fig. 1(a)] and it is available at any desired time. The tangential electric field in the antenna aperture S_a is denoted by $\boldsymbol{E}_a(\boldsymbol{\rho}, t)$, $\boldsymbol{\rho} \in S_a$. The calculation of the radiated field outside the aperture S_a, at any observation point of coordinate $\boldsymbol{r} = (r, \theta, \phi)$ ($\boldsymbol{r} = 0$ being the aperture center) in the half-space $z > 0$, is reduced to the simplified problem of transient radiation from the equivalent magnetic source $\boldsymbol{M}_a(\boldsymbol{\rho}, t) = \boldsymbol{E}_a(\boldsymbol{\rho}, t) \times \hat{\boldsymbol{z}}$ placed over an infinite screen [Fig. 1(b)] in $z = 0$. The magnetic source retains the wedge-effect behavior since it has been computed starting from the real structure. The field outside the aperture is neglected and therefore the simplified model is exact for waveguide-fed screens and

Manuscript received June 11, 2003; revised October 2, 2003. This work was supported in part by the Italian Research Project PRIN-01.

G. Marrocco is with the Dipartimento di Informatica Sistemi e Produzione, Università di Roma Tor Vergata, 00133 Roma, Italy (e-mail: marrocco@disp.uniroma2.it).

M. Ciattaglia is with the Dipartimento di Informatica Sistemi e Produzione, Università di Roma Tor Vergata, 00133 Roma, Italy and also with Alenia Marconi Systems, 00131 Roma, Italy.

Digital Object Identifier 10.1109/TAP.2004.834137

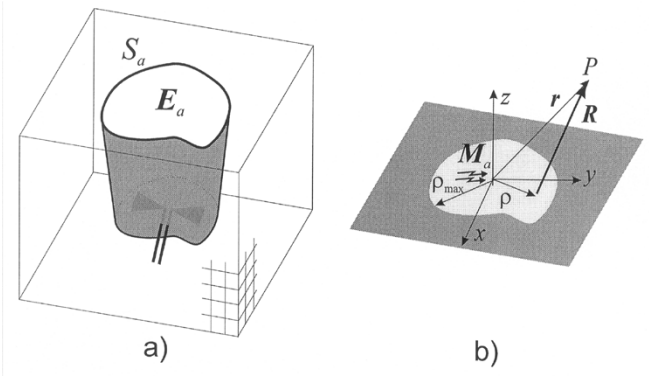

Fig. 1. Strategy for aperture-antenna modeling: (a) the aperture field $\boldsymbol{E}_a(\boldsymbol{\rho},t)$ is computed by a local method applied to a limited space region; (b) the aperture radiation is calculated for the simplified model of an equivalent magnetic source $\boldsymbol{M}_a(\boldsymbol{\rho},t)=\boldsymbol{E}_a(\boldsymbol{\rho},t)\times\hat{\boldsymbol{z}}$ on an infinite screen.

for slots over infinite ground, but it is expected to give approximate results for horns and open-ended waveguides radiating in the free space.

By application of the image principle and the conventional retarded potential theory as described in [2] the transient radiated field is given by

$$\boldsymbol{E}(\boldsymbol{r},t)= \frac{1}{2\pi}\int\!\!\int_{S_a}\hat{\boldsymbol{R}}\times\left(\frac{1}{R^2}+\frac{1}{cR}\frac{\partial}{\partial t}\right)\left[\boldsymbol{E}_a\left(\boldsymbol{\rho},t-\frac{R}{c}\right)\times\hat{\boldsymbol{z}}\right]\boldsymbol{d\rho} \quad (1)$$

with $\boldsymbol{R}=\boldsymbol{r}-\boldsymbol{\rho}$. The retarded time $t-R/c$ accounts for the finite propagation speed c of the field disturbance coming from the aperture.

The dependence on space and time is in general not separable and hence the integral in (1) needs to be evaluated at each observation point and at each time t and a great numerical effort is required for field computation over long times and wide spatial ranges.

III. Data-Fitting for the Aperture Field

To greatly simplify the numerical processing of the radiated field, we introduce a two-step data-fitting model [7], with the aim to approximate the aperture field by means of summation of simple space- and time-variant functions with proper coefficients.

A. Fitting of $\boldsymbol{E}(\boldsymbol{r},t)$ by Space-Varying Functions

At each time t the aperture field is approximated on a set of $\{\boldsymbol{e}_p\}$ time-independent orthogonal vectors

$$\boldsymbol{E}_a(\boldsymbol{\rho},t)\simeq\sum_{p=1}^{N}v_p(t)\boldsymbol{e}_p(\boldsymbol{\rho}) \quad (2)$$

where the time-variant fitting coefficients $\{v_p(t)\}$ are defined as

$$v_p(t)=\int\!\!\int_{S_a}\boldsymbol{E}_a(\boldsymbol{\rho},t)\cdot\boldsymbol{e}_p(\boldsymbol{\rho})\boldsymbol{d\rho}. \quad (3)$$

Several options are possible for the choice of functions $\{\boldsymbol{e}_p\}$. For instance, scalar Spheroidal basis functions, mathematically accounting for the aperture wedge effects, have been proposed in [9]; aperture eigenmodes, known in numerical form and originating from the application of singular expansion method (SEM) theory to the method of moments [10], [11] has permitted in the past decades to efficiently perform a broadband calculation of electromagnetic penetration through rectangular [12] and circular [13] apertures or to solve the dual problem of scattering from finite plates by means of spectral Fourier transform of SEM eigenmodes. As in the previous work of the authors [7], the basis functions considered in this paper are the transverse eigenvectors of waveguide having cross-section equal to the S_a aperture. This choice has been commonly adopted in mode-matching algorithms for the modeling of waveguide-fed screens [14] as well as horn antennas in open space [15] and of slots in infinite screens viewed as a limiting case of a rectangular waveguide with length approaching to zero [14].

The considered basis functions, although less theoretically rigorous than the SEM eigenmodes, and less efficient in the edge-effect modeling than the spheroidal functions, nevertheless possess some useful features when used in conjunction with a numerical FDTD solver. They form a vectorial basis and therefore only scalar expansion coefficient $\{v_p(t)\}$ need to be stored. Additionally, unlike the SEM eigenmodes which are known numerically, this set of functions is available in closed form, at least for canonical cross-sections (rectangular and circular apertures) and originates expansion integrals in (3) suited to fast numerical computation. However, because of the poor fitting of the aperture field discontinuity (at least by means of a small number of modes), an accuracy loss in the low observation angle region is expected as previously discussed in [16] and in [7].

B. Fitting of $v_p(t)$ by Time-Varying Functions

Provided that the antenna is sourced by a finite-duration signal, the aperture field is expected to exhibit damping oscillations related to the field bouncing within the antenna guiding section (internal region) and to the aperture discontinuity. As proposed in [17], the following fitting model is here considered:

$$v_p(t)=f_p(t)+\sum_{k=-K_p}^{K_p}a_{pk}e^{s_{pk}t}U(t) \quad (4)$$

where $U(t)$ is the Heaviside function, and s_{pk} (in [s^{-1}]) and a_{pk} (in [V]) are the complex poles and residues of the exponential functions. From the SEM theory [11] it is known that the representation in terms of complex exponentials with constant coefficients is poorly suited to the early time where local features provide the dominant influence in the scattering phenomena and therefore a nonpole "entire function" $f_p(t)$ needs to be included. Numerous papers investigated the nature of the entire function [10], [18] and the best way to embed its effect into modified exponential coefficients [19]. To easily perform the numerical fitting, we neglect the entire function, as in [20], and we approximate $v_p(t)$ even in the very early transient by only complex exponential terms. As it will be shown in the examples, this approximation still gives high accuracy provided that a reasonable (not too large) number of exponentials is considered in (4).

IV. Approximate Field Transformation

By introducing (2) and (4) in (1), and observing the radiated field after turn-on time $t_r = \max_\rho(R/c)$, e.g., when the whole aperture starts to contribute to the radiation integral, the Heaviside function can be dropped and the field is given by the superposition of pk–contributes with factorized temporal and spatial dependences

$$\boldsymbol{E}(\boldsymbol{r},t) = \frac{1}{2\pi}\sum_{p,k} a_{pk} e^{s_{pk}t} \int\int_{S_a} \left(\frac{1}{R^2} + \frac{s_{pk}}{cR}\right) \times \hat{\boldsymbol{R}} \times [\boldsymbol{e}_p(\boldsymbol{\rho}) \times \hat{\boldsymbol{z}}]\, e^{-(s_{pk}/c)R} d\boldsymbol{\rho}. \quad (5)$$

The interesting advantages of (5) over the global transformation of (1) are that the integral depends only on the observation point, and hence it can be calculated once and for all and then reused for any time t. The whole transient propagation phenomenology is therefore described by $\{s_{pk}\}$ and $\{a_{pk}\}$ sets, which will be later on shown to be small.

An even more attractive feature of the space-time fitting becomes apparent in the far field approximation of (5). Beyond a distance r_F from the aperture given by the Fraunhofer condition $(2\rho_{\max})^2/r_F \ll cT_0$ [21], $\rho_{\max}$ being the maximum distance of source points from the aperture center, and T_0 the time duration of the antenna excitation signal, the factor $1/R$ is approximated by $1/r$ while the standard first-order Taylor expansion $R \simeq r - \boldsymbol{\rho}\cdot\hat{\boldsymbol{r}}$ is adopted for the exponential argument: $e^{-s_{pk}R/c} \simeq e^{-s_{pk}r/c} e^{s_{pk}\hat{\boldsymbol{r}}\cdot\boldsymbol{\rho}/c}$. The turn-on time becomes $t_r = (r + \rho_{\max})/c$. The radiated field, corresponding to each s_{pk} pole, therefore becomes

$$\boldsymbol{E}_{pk}(\boldsymbol{r},t) = \frac{1}{2\pi c r} a_{pk} s_{pk} e^{s_{pk}(t - r/c)} \hat{\boldsymbol{r}} \times \int\int_{S_a} \boldsymbol{e}_p(\boldsymbol{\rho}) e^{(s_{pk}/c)\hat{\boldsymbol{r}}\cdot\boldsymbol{\rho}} d\boldsymbol{\rho} \times \hat{\boldsymbol{z}}. \quad (6)$$

Denoting with $\boldsymbol{F}_{t,p}(\theta,\phi,\omega) = \int\int_{S_a} \boldsymbol{e}_p(\boldsymbol{\rho}) e^{j(\omega/c)\hat{\boldsymbol{r}}\cdot\boldsymbol{\rho}} d\boldsymbol{\rho}$ the asymptotic transverse component of the pth *modal space factor* [7], e.g., the spectral Fourier transform of the pth aperture field pattern, it is immediate to recognize that the integral in (6) is directly obtained from the modal space factor when ω is replaced by $-js_{pk}$. By recalling that $\boldsymbol{F}_p = \boldsymbol{F}_{t,p} - \tan\theta(F_{x,p}\cos\phi + F_{y,p}\sin\phi)\hat{\boldsymbol{z}}$ and the far field property $\hat{\boldsymbol{r}}\cdot\boldsymbol{F}_p = 0$ [22], after simple vectorial manipulations the following expression can be derived for the electric far field radiated by the pth aperture field pattern $\boldsymbol{E}_{a,p}(\boldsymbol{\rho},t) = v_p(t)\boldsymbol{e}_p(\boldsymbol{\rho})$

$$\boldsymbol{E}_p(\boldsymbol{r},t) = \frac{1}{2\pi r c}\cos\theta \sum_k s_{pk} a_{pk} \boldsymbol{F}_{pk}(\theta,\phi) e^{s_{pk}(t - r/c)} \quad (7)$$

valid for $t \geq t_r$, where $\boldsymbol{F}_{pk}(\theta,\phi) = \boldsymbol{F}_p(\theta,\phi,-js_{pk})$. Provided that the modal space factor may be computed in closed form, transient field can be generated by (7) without numerical solution of any integral.

The approximated expression in (7) has an interesting relationship with the exact formulation in [21] and [23] involving the slant stack transform (SST) of the aperture field $\tilde{\boldsymbol{E}}(\boldsymbol{r},t) = \int\int_{S_A} \boldsymbol{E}_a(\boldsymbol{\rho}, t + \hat{\boldsymbol{r}}\cdot\boldsymbol{\rho}/c) d\boldsymbol{\rho}$, based on the Radon transform. According to this theory, the electric far field radiated by each $\boldsymbol{E}_{a,p}(\boldsymbol{\rho},t)$ is expressed as $\boldsymbol{E}_p(\boldsymbol{r},t) = (1/2\pi rc)\cos\theta(\partial/\partial t)\tilde{\boldsymbol{E}}_p(\boldsymbol{r}, t - r/c)$. Since the SST is the inverse Fourier transform of the aperture plane-wave spectrum in asymptotic evaluation, e.g., $\tilde{\boldsymbol{E}}_p(\boldsymbol{r},t) = \mathcal{F}^{-1}\left[\int\int_{S_A} \hat{\boldsymbol{E}}_{a,p}(\boldsymbol{\rho},\omega) e^{j\boldsymbol{k}\cdot\boldsymbol{\rho}} d\boldsymbol{\rho}\right]\Big|_{\boldsymbol{k}=k_0\hat{\boldsymbol{r}}}$ ($\hat{\boldsymbol{E}}_a(\boldsymbol{\rho},\omega)$ being the ω-Fourier transform of the pth aperture field), therefore it is easy to see that (7) can be considered as originating from the exact far field formula when the SST of the pth aperture field pattern is approximated by the discrete inverse Fourier transform of the pth plane-wave spectrum at complex frequencies $\omega_k = -js_{pk}$. As a consequence, the angular spreading $\boldsymbol{F}_{pk}\cos\theta$ is formally independent on t variable and it is only affected by the modal pattern order p and by the pole s_{pk} (which, however, gives an implicit time dependence). The SST formulation accurately describes the early transient and it is a true time-domain transform, nevertheless it requires the numerical evaluation of integrals with coupled space and time variables. Moreover, although it does not possess the same true physical meanning, expression (7) is formally similar to a far field natural mode [19] originated from the more rigorous SEM theory.

Since modal voltages $\{v_p(t)\}$ are real- valued signals, poles and residues come in conjugate pairs: $s_{p,-k} = s_{pk}^*$ and $a_{p,-k} = a_{pk}^*$ ("*" denoting complex conjugate). Accordingly, real valued radiated modal fields can be obtained by pairing $\boldsymbol{E}_{pk} + \boldsymbol{E}_{p,-k} \equiv \boldsymbol{\mathcal{E}}_{pk}$, $k = 0 \ldots K_p$, as it will be shown with more details in the next sessions for the particular cases of rectangular and circular apertures.

A. Modal Space Factors for Rectangular Apertures

For rectangular apertures of $a \times b$ sides, the transverse component of modal space factor, as obtained in [7] is, for TE_{mn} eigenvectors

$$\boldsymbol{F}_{t,mn} = -4(j)^{m+n-1} T_{mn} \frac{\sin\left(\frac{k_x a + m\pi}{2}\right)}{(k_m^2 - k_x^2)} \cdot \frac{\sin\left(\frac{k_y b + n\pi}{2}\right)}{(k_n^2 - k_y^2)} \begin{bmatrix} k_n^2 k_x \hat{\boldsymbol{x}} \\ -k_m^2 k_y \hat{\boldsymbol{y}} \end{bmatrix} \quad (8)$$

with $k_m = m\pi/a$, $k_n = n\pi/b$, $k_x = k_0 r_x$, $k_y = k_0 r_y$, $r_x = \hat{\boldsymbol{x}}\cdot\hat{\boldsymbol{r}}$, $r_y = \hat{\boldsymbol{y}}\cdot\hat{\boldsymbol{r}}$ and T_{mn} is a normalization factor. Similar expressions hold for TM modes with $F_{x,mn}^{\mathrm{TM}} = -(k_m/k_n)F_{x,mn}^{\mathrm{TE}}$ and $F_{y,mn}^{\mathrm{TM}} = (k_n/k_m)F_{y,mn}^{\mathrm{TE}}$.

By taking into account the substitution of ω with $-js_{pk}$ and by using the properties $\sin(jz) = j\sinh z$ the modal space factor in spherical coordinates becomes

$$\boldsymbol{F}_{mnk} = -(j)^{m+n}\varphi_{mnk} \begin{bmatrix} \frac{k_n^2 r_x \cos\phi - k_m^2 r_y \sin\phi}{\cos\theta}\hat{\boldsymbol{\theta}} \\ -(k_n^2 r_x \sin\phi + k_m^2 r_y \cos\phi)\hat{\boldsymbol{\phi}} \end{bmatrix} \quad (9)$$

where

$$\varphi_{mnk} = 4(ab)^2 \frac{s_{mnk}}{c} T_{mn} \frac{\sinh\left(\frac{u_{mnk}}{2} + j\frac{m\pi}{2}\right)}{[u_{mnk}^2 + (k_m a)^2]} \cdot \frac{\sinh(\frac{v_{mnk}}{2} + j\frac{n\pi}{2})}{[v_{mnk}^2 + (k_n b)^2]} \quad (10)$$

with $u_{mnk} = s_{mnk} r_x a/c$ and $v_{mnk} = s_{mnk} r_y b/c$. Real-valued radiated modal field $\boldsymbol{\mathcal{E}}_{mnk} = \boldsymbol{E}_{mnk} + \boldsymbol{E}_{mn,-k}$ can be obtained

by the property $\sinh(z^*+jm\pi/2) = (-1)^m \sinh^*(z+jm\pi/2)$ which permits to calculate $\varphi_{mn,-k} = (-1)^{m+n}\varphi^*_{mnk}$ and finally

$$\boldsymbol{\mathcal{E}}_{mnk}(\boldsymbol{r},t) = (-1)^{(m+n+3-q)/2}|A_{mnk}(\theta,\phi)|\frac{e^{-\alpha_{mnk}(t-r/c)}}{\pi rc}\cdot \cdot \sin\left[\omega_{mnk}\left(t-\frac{r}{c}\right)+\Phi_{mnk}(\theta,\phi)-\frac{q\pi}{2}\right]\cdot \cdot \begin{bmatrix}(k_n^2 r_x\cos\phi - k_m^2 r_y \sin\phi)\hat{\boldsymbol{\theta}} \\ -(k_n^2 r_x \sin\phi + k_m^2 r_y\cos\phi)\cos\theta\hat{\boldsymbol{\phi}}\end{bmatrix},\ t > t_r \tag{11}$$

where we have posed $s_{mnk} = -\alpha_{mnk} + j\omega_{mnk}$, $\varphi_{mnk}(\theta,\phi)a_{mnk}s_{mnk} = |A_{mnk}(\theta,\phi)|e^{j\Phi_{mnk}(\theta,\phi)}$ and $q = 1$ or 0 for even or odd $(m+n)$, respectively.

It is worth noticing that the contribute of each pole to the radiated real-valued field still shows a damped sinusoidal dependence. The field attenuates along with the distance and with time according to the pole real part. The amplitude and the oscillating phase depend on the observation points and on the pole. Nevertheless, the full separability of temporal and spatial variables is lost when moving from a complex representation $\boldsymbol{E}_{mnk}$ to real-valued $\boldsymbol{\mathcal{E}}_{mnk}$.

B. Modal Space Factors for Circular Apertures

For circular aperture antennas of radius A, the computation of pattern space factors can be derived from [24]

$$\begin{aligned}\boldsymbol{F}_{mn}(k_0,\theta,\phi) &= -j2\pi AT_{mn}\left\{\frac{1}{\cos\theta}\left[b_{mn}j^m m J_m(p'_{mn})\frac{J_m(u)}{u}\right.\right. \\ &\quad \left.\left. -(b_{mn}-1)j^m p_{mn}J'_m(p_{mn})\frac{uJ_m(u)}{p_{mn}^2-u^2}\right]\sin m\phi\hat{\boldsymbol{\theta}} + \right. \\ &\quad \left. + \left[b_{mn}j^m p'^2_{mn}J_m(p'_{mn})\frac{J'_m(u)}{p'^2_{mn}-u^2}\right]\cos m\phi\hat{\boldsymbol{\phi}}\right\}\end{aligned} \tag{12}$$

with $u = k_0 A\sin\theta$, $b_{mn} = \begin{cases}1 & \text{TE}\\ 0 & \text{TM}\end{cases}$, T_{mn} is a normalization constant, p_{mn} the nth zero of Bessel function J_m and p'_{mn} the nth zero of its first derivative. Substitution of ω with $-js_{mnk}$ (and therefore $u_{mnk} = -j(s_{mnk}/c)A\sin\theta$) gives the radiated TE modal field

$$\begin{aligned}E_{mnk,\theta} &= L_{mnk}\frac{e^{s_{mnk}(t-r/c)}}{r}\frac{\sin m\phi}{\sin\theta}J_m(u_{mnk})U\left(t-\frac{r}{c}\right) \\ E_{mnk,\phi} &= M_{mnk}\frac{e^{s_{mnk}(t-r/c)}}{r}\cos m\phi\cos\theta\cdot \\ &\quad \cdot\frac{J'_m(u_{mnk})}{p'^2_{mn}-u^2_{mnk}}U\left(t-\frac{r}{c}\right)\end{aligned} \tag{13}$$

with $M_{mnk} = -j^{m+1}s_{mnk}a_{mnk}/cAT_{mn}p'^2_{mn}J_m(p'_{mn})$, and $L_{mnk} = mj^m T_{mn}s_{mnk}a_{mnk}/cJ_m(p'_{mn})$. The property $J_m(-jz^*) = (-1)^m J^*_m(-jz)$ permits to obtain a real-valued expression similar to (11). The extension to TM is straightforward.

V. Implementation of the Method

The FDTD solver performs a fullwave analysis of the whole antenna including a small portion of the external free-space [see Fig. 1(a)] in the close surrounding of the aperture. In this case, the computed aperture field will account for the edge effect. The modal amplitudes $\{v_p(t)\}$ for the considered basis functions $\{\boldsymbol{e}_p\}$ are computed "at run-time" by discretization, on the FDTD grid and at times $t_n = n\Delta t$ (Δt being the FDTD time step), of the internal product in (3). Details and guidelines for numerical implementation of (3) have been discussed in [7] and [25]. In particular, only those modes with cutoff frequency $f_{mn} \le f_{\max}$ will be considered, with $f_{\max}$ the maximum frequency of the source signal.

Time-variant coefficients $\{v_p(t_n)\}$ are then used to estimate the parameters $\{a_{pk}, s_{pk}\}$ of each mode by the Matrix Pencil method [26]. Additionally, to prevent instabilities, the unstable poles ($\mathrm{Re}[s_{pk}] > 0$) are pruned and the corresponding residues a_{pk} are obtained by means of least square optimization.

The set of poles and residues to be really retained and stored for the calculation of the radiated field can be further thinned according to the strength of the *energy* indicator ξ_{pk} associated to each pkth pole

$$\xi_{pk} = \int_0^\infty |a_{pk}e^{s_{pk}t}|^2 dt. \tag{14}$$

Computation of (7) will be therefore restricted to those poles, among all the $\{s_{pk}\}$, whose energy ξ_{pk} is such that $\xi_{pk}/\xi_{\max} \ge \varepsilon$, where ε is a threshold and $\xi_{\max} = \max_{pk}\{\xi_{pk}\}$. Guidelines about how to choose the threshold will be discussed in the next section.

VI. Numerical Results

The method has been validated by application to a rectangular slot on a metal plate and to a true ultrawide-band circular ridged horn. Far fields obtained by the new method (hereafter labeled as $\boldsymbol{E}^{\mathrm{N2F}}$) have been compared with reference solutions obtained by an independent FDTD simulation (labeled as $\boldsymbol{E}^{\mathrm{FDTD}}$) whose computational domain is large enough to include some far field test points in front of the aperture.

The comparisons will be characterized by the correlation coefficient or *Fidelity* indicator [27]

$$\rho_F(s_1,s_2) = \max_\tau \frac{\int_0^{+\infty} s_1(t+\tau)\,s_2(t)\,dt}{\sqrt{\int_0^{+\infty}|s_1(t)|^2dt\cdot\int_0^{+\infty}|s_2(t)|^2dt}} \tag{15}$$

where s_1 and s_2 are the electromagnetic fields (at a same point) to be compared, the parameter τ is the time shift which maximizes ρ_F and the integrals are computed as finite summations respect to time samples t_n.

A. Rectangular Slot on a Metal Screen

A rectangular $a \times b$ slot on a 1 cm thick perfect electric screen [6] is excited by a dipole placed in front of the aperture (Fig. 2). The structure has been meshed on a nonuniform rectangular FDTD grid with voxel size $0.5\ \mathrm{cm} \le \Delta x, \Delta y, \Delta z \le 1.5\ \mathrm{cm}$ and U-PML boundary conditions [28] truncate the computational domain. The dipole has been sourced by a Gaussian

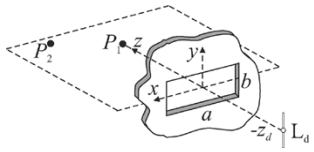

Fig. 2. Dipole-sourced rectangular slot on an infinite ground plane. Size (in centimeters): $a = 10, b = 5, L_d = 11.5, z_d = 8$.

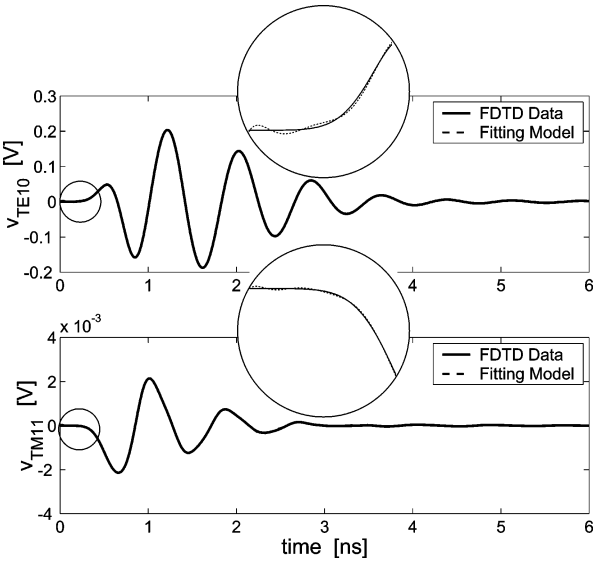

Fig. 3. Fitting of slot modal voltages $v_{\mathrm{TE}_{10}}(t)$ and $v_{\mathrm{TM}_{11}}(t)$ by means of (4) with eight and 11 poles, respectively. The very early transient is magnified within circles.

voltage generator $v_0(t) = V_g e^{(t-t_0)^2/2T^2}$ with parameters $V_g = 1\,\mathrm{V}, T = 0.126\,\mathrm{ns}$ and $t_0 = 0.714\,\mathrm{ns}$ such to provide a $-3\,\mathrm{dB}$ bandwidth of [0–2.8 GHz], e.g., $V_0(2.8\,\mathrm{GHz}) = 1/\sqrt{2}V_0(0)$ and $V_0(f)$ the Fourier transform of $v_0(t)$. According to the size of the aperture, the Fraunhofer distance, for $T_0 = 4T$, is $r_F = 33\,\mathrm{cm}$ and the proposed method has been applied for times $t - r/c > \sqrt{a^2+b^2}/2c = 0.18\,\mathrm{ns}$.

Time-variant coefficients $\{v_p(t)\}$ of the aperture field space-fitting have been computed according to (3) and then fitted to expression in (4) without the entire function $f_p(t)$. To demonstrate the accuracy of this fitting model, even in the early transient, the fitted amplitudes of TE_{10} ($v_{\mathrm{TE}_{10}}$) and TM_{11} ($v_{\mathrm{TM}_{11}}$) modes, obtained by Matrix Pencil with 8 and 11 exponential terms respectively, are shown in Fig. 3. A pretty good agreement can be appreciated in the whole time scale with fidelity $\rho_F = 0.9999$ (TE_{10}) and $\rho_F = 0.9998$ (TM_{11}).

Because of the amplitude $v_{10}(t)$ of the TE_{10} mode (cutoff frequency $f_{mn} = 1.5\,\mathrm{GHz}$) is much more excited than that of the other considered modes, only poles-residues of $v_{10}(t)$ have been retained for the far field computation. In Fig. 4, snapshots of the electric field E_ϕ on the H-cut, are presented at different times. The wavepacket tail, due to the slot diffraction, is clearly visible.

Fig. 5 shows the transient far field at point P_1 on the antenna axis and at point P_2 at angular distance $\theta = 23°$ from the axis. It can be observed that the far fields are correctly predicted by the N2F transformation by means of just three poles corresponding to a threshold $\varepsilon = 10^{-1}$ with a fidelity indicator $\rho_F(E^{\mathrm{FDTD}}, E^{\mathrm{N2F}}) = 0.97$, except for the signals' turn-on where spurious oscillations are visible. Nine poles ($\varepsilon = 10^{-3}$)

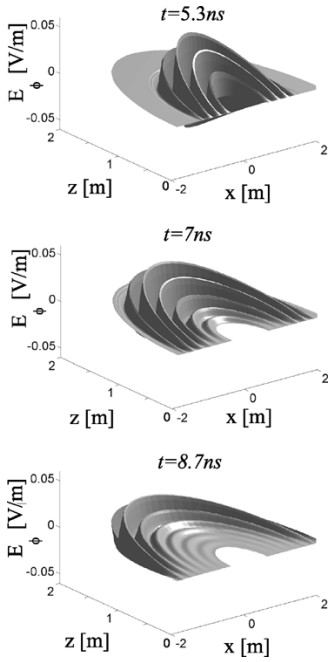

Fig. 4. Radiation from a dipole-sourced rectangular slot on an infinite ground plane, for different times and for $r > 0.5\,\mathrm{m}$.

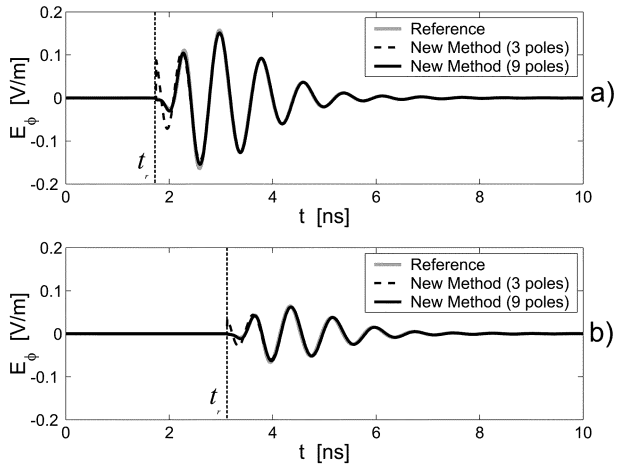

Fig. 5. Transient radiated electric field (ϕ component) from the rectangular slot at (a) on-axis point $\mathrm{P}_1 = (r_1 = 35\,\mathrm{cm}, \theta_1 = 0°, \phi_1 = 0°)$ (see Fig. 2) and (b) at off-axis point $\mathrm{P}_2 = (r_2 = 76\,\mathrm{cm}, \theta_2 = 23°, \phi_2 = 0°)$ as computed by full FDTD model (reference) and generated by means of the new method for $t > t_r$ with the only TE_{10} mode, and poles corresponding to $\varepsilon = 10^{-1}$ and $\varepsilon = 10^{-3}$ thinning thresholds.

give an almost full coincidence with the reference solution, yielding a fidelity $\rho_F = 0.99$.

B. Circular Ridged Horn

A circular ridged horn (CRH) antenna, originally developed by SMA for microwave hypertermia [29] and commonly used as TD measurement probe [30] **,** is sourced by a coaxial probe (Fig. 6). The antenna frequency band is 4–10 GHz. At purpose of application of the new method, a 25 cm × 25 cm × 45 cm region, including the antenna and a small air region in front of the aperture, has been meshed on a cubic FDTD grid with size $\Delta = 3\,\mathrm{mm}$ for overall $83 \times 84 \times 199$ voxels. The coaxial probe has been sourced by a Gaussian voltage generator with parameters $T = 35\,\mathrm{ps}$ and $t_0 = 200\,\mathrm{ps}$ such to provide a

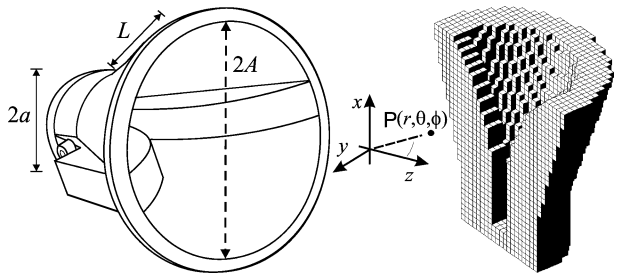

Fig. 6. Circular ridged horn for 4 GHz – 10 GHz frequency band. Sizes (in centimeters): $A = 3.6$, $a = 1.8$, $L = 6$; FDTD model on a cubic grid (half the geometry has been removed for clarity).

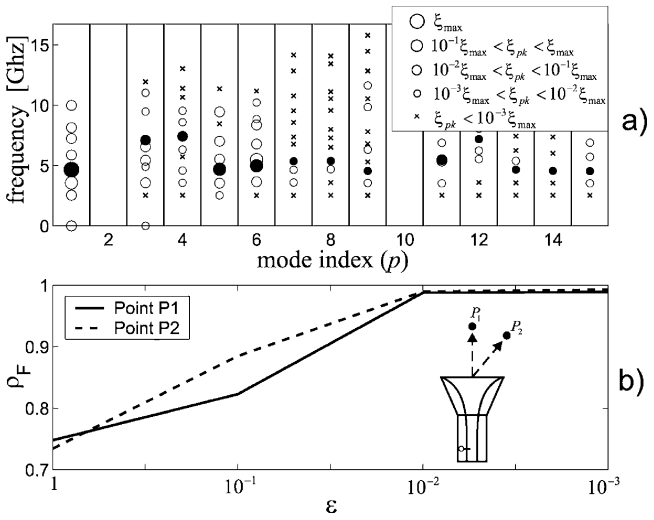

Fig. 7. (a) Spectrum of the aperture field for the CRH antenna. Circles represent the s_{pk}'s energy. Modes are sorted in ascending order by the index $p = (m, n)$ according to their cutoff frequency. The ordinate axis represents the pole resonance $\omega_{pk}/(2\pi)$. Filled circles tag poles with the highest energy for each mode p. (b) Fidelity indicator $\rho_F(E^{\mathrm{FDTD}}, E^{\mathrm{N2F}})$ vs. the threshold ε at the observation points $\mathrm{P}_1(\mathrm{r}_1 = 15\ \mathrm{cm}, \theta_1 = 0°, \phi_1 = 0°)$ and $\mathrm{P}_2(\mathrm{r}_2 = 50\ \mathrm{cm}, \theta_1 = 17.7°, \phi_1 = 45°)$.

-3 dB bandwidth of [0–10 GHz]. The Fraunhofer distance is $r_F = 12.3$ cm and the proposed method has been applied for times $t - r/c > 0.12$ ns.

Twenty circular waveguide modes, with cutoff frequency $f_{mn} \leq 10$ GHz have been considered on the aperture. The pole distribution is shown in Fig. 7(a), with indication of the corresponding energy ξ_{pk} (p being a sorting parameter over (m, n)–modes). It can be observed that only ten poles have energy more than the 10% ($\varepsilon = 10^{-1}$) of the maximum (corresponding to the $s_{1,15}$ pole of the TE_{11} voltage amplitude). The fidelity between the full-FDTD solutions (E_ϕ field) and new method's outcomes is shown in Fig. 7(b). No valuable improvement in the fidelity is achieved imposing a threshold smaller than 10^{-2} and this can be a reasonable guideline for the pole thinning. As an example, the transient far field generated by the new method for threshold $\varepsilon = \{10^{-1}, 10^{-2}, 10^{-3}\}$ is presented in Fig. 8. A good agreement can be appreciated both in the early transient and in the signal tail provided that $\varepsilon \leq 10^{-2}$. Moreover, no visible difference is apparent by the use of more than 30 poles. In Fig. 9, snapshots of the electric field E_ϕ on the H-cut are presented at different times. Due to the broadband features of the CRH antenna, the Gaussian

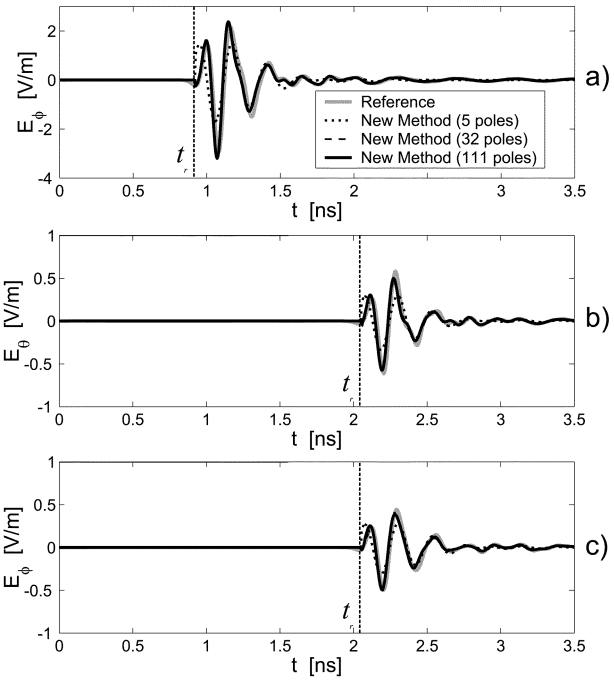

Fig. 8. Transient radiated electric field from CRH antenna computed by full FDTD model (reference) and generated by means of different numbers of poles corresponding to $\varepsilon = 10^{-1}, \varepsilon = 10^{-2}$ and $\varepsilon = 10^{-3}$; (a) E_ϕ at point P_1, (b) E_θ at point P_2, c) E_ϕ at point P_2.

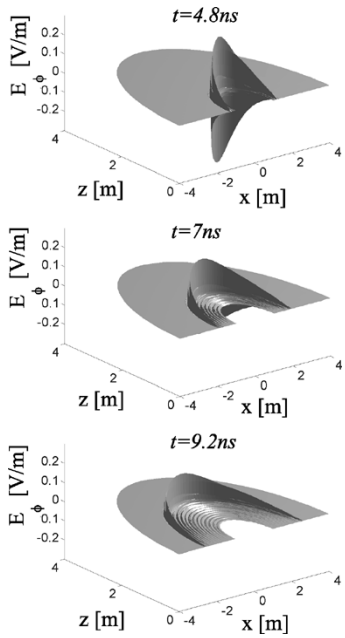

Fig. 9. Snapshots of CRH far field E_ϕ on the H-cut, computed by the new method at different times for $r > 1$ m.

pulse propagates with small oscillations in the tail. The spatial compact localization of the wavepacket indicates the higher gain of the CRH antenna compared with the slot of the previous example.

VII. Conclusion

A two-step data-fitting of the aperture field, by means of interpolating functions with uncoupled time and space variables,

has permitted to efficiently calculate the transient far field radiated by aperture-type antennas. The relevant propagation phenomenology is described, with good approximation in both spatial and temporal scale, by storing a few time-independent complex numbers (poles and residues), related to the antenna geometrical and electrical complexity as well as to the analysis bandwidth. In particular, less than 10 poles-residues couplets have been required for the modeling of a slot antenna, while about 30 couplets have been considered in the case of a more complex circular ridged horn.

The method is a true off-line procedure and much more than a simple field compression option of the transient aperture field since the evaluation of radiation integrals benefits from the specific form of the fitting functions. The computer time required to perform aperture field expansion is negligible in comparison with those of typical FDTD runs or of conventional N2F transformations. By taking advantage from data reusability, transient field distribution over wide scan angles can be computed in seconds over medium power personal computers.

REFERENCES

[1] R. J. Fontana, "Recent applications of ultra-wideband radar and communications systems," in *Ultra-Wideband Short-Pulse Electromagnetics*, P.D. Smith and S.R. Cloude, Eds. Norwell, MA/New York: Kluwer/Plenum, 2000, vol. 5, pp. 225–234.

[2] A. Taflove, *Computational Electromagnetics: The Finite Difference Method*. Norwood, MA: Artech House, 1995.

[3] K. A. Remley, A. Weisshar, S. M. Goodnick, and V. K. Tripathi, "Characterization of near- and far-field radiation from ultrafast electronic systems," *IEEE Trans. Microwave Theory Tech.*, vol. 46, pp. 2476–2483, Dec. 1998.

[4] C. Oetting and L. Klinkenbusch, "Improving the accuracy of numerical results by a spherical-multipole based post-processing," in *Proc. IEEE AP-S Int. Symp.*, San Antonio, TX, 2002, pp. 44–47.

[5] I. J. Craddock, P. G. Turner, and C. J. Railton, "Reducing the computational overhead of the near-field transform through system identification," *Electron. Lett.*, vol. 30, pp. 1609–1610, 1994.

[6] D. Sullivan and J. L. Young, "Far-field time-domain calculation from aperture radiators using the FDTD method," *IEEE Trans. Antennas Propagat.*, vol. 49, pp. 464–469, Mar. 2001.

[7] G. Marrocco, "Modal near-field to far-field transformation for FDTD modeling of aperture antennas," *J. Electromagn. Waves Appl.*, vol. 17, pp. 79–98, 2003.

[8] G. Marrocco and M. Ciattaglia, "Broadband modeling of waveguide antennas by a combined FDTD and modal-N2F method," in *Proc. Applied Computational Electromagnetics Conf.*, Monterey, CA, 2003, pp. 217–222.

[9] D. R. Rhodes, *Synthesis of Planar Antenna Sources*. Oxford, U.K.: Clarendon Press, 1974.

[10] C. E. Baum, "The singularity expansion method," in *Transient Electromagnetic Fields*, L.B. Flesen, Ed. Berlin: Springer-Verlag, 1976, pp. 129–179.

[11] ——, "Toward an engineering theory of electromagnetic scattering: The singulariry and eigenmode expansion methods," in *Electromagnetic Scattering*, P. L. E. Uslenghi, Ed. New York: Academic Press, 1978, pp. 571–651.

[12] L. W. Pearson and R. Mittra, "The singularity expansion representation of the transient electromagnetic coupling through a rectangular aperture," in *Interaction Notes*, June 1976, Note 296.

[13] C. D. Taylor, T. T. Crow, and K. T. Chen, "On the singularity expansion method applied to aperture penetration: Part I Theory," in *Interaction Notes*, May 1973, Note 134.

[14] B. N. Das, A. Chakraborty, and S. Gupta, "Analysis of waveguide-fed thick radiating rectangular windows in a ground plane," *Proc. Inst. Elect. Eng. Microwaves, Antennas and Propagation*, vol. 138, no. 2, pp. 142–146, 1991.

[15] R. Bunger, R. Beyer, and F. Arndt, "Rigorous combined mode-matching integral equation analysis of horn antennas with arbitrary cross section," *IEEE Trans. Antennas Propagat.*, vol. 47, pp. 1641–1648, Nov. 1999.

[16] A. Q. Howard Jr, "A comparison of mode match, geometrical theory of diffraction and Kirchhoff radiation," *IEEE Trans. Antennas Propagat.*, vol. AP-21, pp. 100–102, 1973.

[17] E. K. Miller, "Model-based parameter estimation in electromagnetics: Part I. Background and theoretical development," *IEEE Antennas Propagat. Mag.*, vol. 40, pp. 42–52, Feb. 1999.

[18] E. Heyman and L. B. Felsen, "A wavefront interpretation of the singular expansion method," *IEEE Trans. Antennas Propagat.*, vol. AP-33, pp. 706–718, 1985.

[19] L. W. Pearson, "A note on the representation of scattered fields as a singular expansion," *IEEE Trans. Antennas Propagat.*, vol. AP-32, pp. 520–524, 1984.

[20] A. Poggio, M. VanBlaricum, E. Miller, and R. Mittra, "Evaluation of a processing technique for transient data," *IEEE Trans. Antennas Propagat.*, vol. AP-26, pp. 165–173, Jan. 1978.

[21] A. Shlivinski, E. Heyman, and R. Kastner, "Antenna characterization in the time domain," *IEEE Trans. Antennas Propagat.*, vol. 45, pp. 1140–1149, July 1997.

[22] C. Balanis, *Antenna Theory, Analysis and Design*. New York: Wiley, 1997.

[23] T. B. Hansen and A. D. Yaghjian, "Planar near-field scanning in the time domain, Part 1: Formulation," *IEEE Trans. Antennas Propagat.*, vol. 42, pp. 1280–1291, Sept. 1994.

[24] A. C. Ludwig, "Radiation pattern synthesis for circular aperture horn antennas," *IEEE Trans. Antennas Propagat.*, vol. AP-14, pp. 434–440, 1966.

[25] G. Marrocco and F. Bardati, "Broadband horn-antenna launchers modeling by FDTD and generalized scattering matrix methods," *IEEE Trans. Antennas Propagat.*, vol. 50, pp. 1688–1696, Dec. 2002.

[26] T. K. Sarkar and O. Pereira, "Using the matrix pencil method to estimate the parameters of a sum of complex exponentials," *IEEE Antennas Propagat. Mag.*, vol. 37, pp. 48–55, Feb. 1995.

[27] D. Lamensdorf and L. Susman, "Baseband-pulse-antenna techniques," *IEEE Antennas Propagat. Mag.*, vol. 36, pp. 20–30, Feb. 1994.

[28] S. D. Gedney, "An anisotropic PML absorbing media for FDTD simulation of fields in lossy dispersive media," *Electromagn.*, vol. 16, pp. 399–415, 1996.

[29] G. A. Lovisolo, M. Adami, G. Arcangeli, and A. Borrani, "A multifrequency water-filled waveguide application thermal dosimetry *in vivo*," *IEEE Trans. Microwave Theory Tech.*, vol. 32, pp. 893–896, Aug. 1984.

[30] W. A. van Cappellen, R. V. der Jongh, and L. P. Ligthart, "Potentials of ultra-short-pulse time-domain scattering measurements," *IEEE Antennas Propagat. Mag.*, vol. 42, pp. 35–45, Feb. 2000.

Gaetano Marrocco (M'98) received the Laurea degree in electronic engineering and the Ph.D. degree in applied electromagnetics from the Universita degli Studi dell' Aquila, L'Aquila, Italy, in 1994 and 1998, respectively.

In summer 1994, he was at the University of Illinois at Urbana-Champaign as a Postgraduate Student. Since 1997, he has been a Researcher at the Università di Roma–Tor Vergata, Roma, Italy, where he currently teaches antenna design. In autumn 1999, he was a Visiting Researcher at the Imperial College, London, U.K. He has been involved in several Space, Avionic and Naval programs of the European Space Agency, NATO, Italian Space Agency, and Italian Navy. His research is mainly directed to the development of numerical methods and signal processing techniques for the time domain modeling of complex electromagnetic structures in the context of biological and aerospace applications.

Matteo Ciattaglia (S'01) received the Laurea degree in telecomunication engineering from the Università di Roma–Tor Vergata, Roma, Italy, in 2002, where he is currently working toward the Ph.D. degree.

In 2003, he was Grant Researcher at theUniversità di Roma–Tor Vergata working on numerical methods for time-domain electromagnetics. He is currently employed at Alenia Marconi Systems, Roma, Italy, working on phased arrays modeling.